Theoret. chim. Acta (Berl.) 28, 267—282 (1973)

Vibronic and Spin-Orbit Splitting in Spectra of Systems Exhibiting Jahn-Teller-Effect

Peter Habitz and Wilhelm Hans Eugen Schwarz
Lehrstuhl für Theoretische Chemie der Universität, Wegelerstr. 12, 53 Bonn, Germany

Received October 6, 1972

Simple two- and three-dimensional models have been used to investigate the vibronic states of molecules exhibiting Jahn-Teller-Effect. According to the topology of the adiabatic potential surface, two cases have to be distinguished, which may (A) or may not (B) be treated in the Born-Oppenheimer approximation. In the latter case B strong Jahn-Teller coupling leads to a splitting of an $A \rightarrow E$ absorption line into three peaks instead of the usual two ones. This additional splitting originates from transitions into the first and second metastable level of the upper potential well. However, the vibronic splitting will often be smeared out by coupling of the Jahn-Teller effect to a distortion of a Jahn-Teller inactive vibration. The effective spin-orbit splitting of an absorption band with unresolved vibrational structure is larger than in the case of vanishing Jahn-Teller coupling, contrary to the spin-orbit splitting of single vibronic levels. An experimental example of this effect is discussed. In Jahn-Teller case B it may be interpreted as a superposition of the vibronic and the spin-orbit splitting effects.

Mittels einfacher zwei- und dreidimensionaler Modelle wurden die vibronischen Zustände von Molekülen untersucht, die einen Jahn-Teller-Effekt zeigen. Entsprechend der Topologie der adiabatischen Potentialfläche sind zwei Fälle A und B zu unterscheiden, die im Rahmen der Born-Oppenheimer-Näherung behandelt werden können bzw. wo dies nicht möglich ist. Im letzteren Falle B führt eine sehr starke Jahn-Teller-Kopplung zur Aufspaltung einer $A \rightarrow E$ Absorptionslinie in drei statt wie üblich in zwei Peaks. Diese zusätzliche Aufspaltung rührt her von Übergängen in die ersten beiden metastabilen Resonanzzustände der oberen Potentialmulde. In vielen Fällen wird mit einer Jahn-Teller-Kopplung der asymmetrischen Schwingung eine Verschiebung der Gleichgewichtslage einer Jahn-Teller inaktiven Schwingung einherlaufen: Die vibronischen Aufspaltungen sollten daher durch Schwingungsverbreiterung teilweise verschmiert sein. Während die Spin-Bahn-Aufspaltung einzelner vibronischer Niveaus durch Jahn-Teller-Kopplung verringert wird, wird die effektive Spin-Bahn-Aufspaltung einer Absorptionslinie mit nichtaufgelöster Schwingungsstruktur vergrößert. Ein experimentelles Beispiel für diesen Effekt wird diskutiert. Im Jahn-Teller-Fall B kann er als Überlagerung der vibronischen und der Spin-Bahn-Aufspaltung interpretiert werden.

1. Introduction

Let us consider a molecule with a degenerate electronic state in the Born-Oppenheimer approximation. Under a symmetry-breaking distortion, the degenerate electronic state will usually split. According to Jahn and Teller [1–3] there exists at least one nontotally symmetric vibrational coordinate, x, for a non-linear molecule M, where the splitting is linear in x. If M is stable against dissociation, the corresponding adiabatic potential curves may be approximated by

$$V(x) = k/2(x \pm R_0)^2 .$$

Now let us consider a second symmetry coordinate y, one which will result in vibrational bands of appreciable intensity. We have to distinguish between

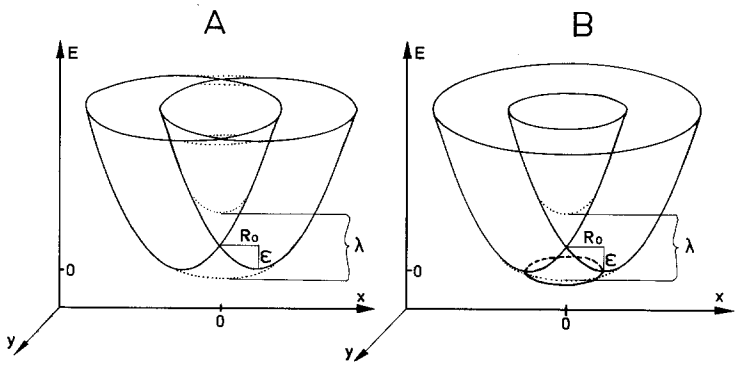

Fig. 1. Potential energy as a function of two symmetry coordinates. Case A: x is Jahn-Teller active, y inactive (two intersecting paraboloids). Case B: both x and y are Jahn-Teller active (only one surface, the Jahn-Teller cone). Dotted lines: an additional spin-orbit coupling leads to two separate adiabatic potential surfaces in both cases

Table 1. Classification of Jahn-Teller effect

Non-linear symmetries with degenerate representations	Degenerate electronic state	Jahn-Teller active symmetry coordinates	Relevant symmetry coordinates	Topology of the corresponding adiabatic potential energy surface
Tetragonal	E	b_1, b_2	one b, one a_1	A
			b_1 and b_2	B
Trigonal, pentagonal, hexagonal	E	e	e	B
Cubic	E	e	e	B
	T	e, t	e	A
			t	B

two possibilities: A) the y-coordinate is Jahn-Teller inactive or B) it is active. These cases A and B differ by the topology of the potential surface as is shown in Fig. 1. Examples of the two cases are given in Table 1. E.g. case A is approximately realized by a doubly degenerate electronic state of a tetragonal molecule, if only vibrations of species a_1 and b_2 are of relevance for the phenomenon to be discussed, i.e. the optical absorption spectrum. The main difference between the two cases is, that the adiabatic surfaces A may be considered as diabatic surfaces, too, whereas this is not possible with the adiabatic surface B. Correspondingly the nuclear motion in case A may be calculated within the Born-Oppenheimer approximation, whereas in case B one has to use at least the diabatic two-state approximation [4], as has been done in the classical works of Longuet-Higgins *et al.* and Ballhausen [5].

2. Calculational Model

In this way we have calculated vibronic energy levels and wave functions. Some details are given in Appendix A, see also Ref. [6]. The following simple adiabatic potential surfaces have been used:

Case A: the two surfaces V_1 and V_2 depend on a one-fold degenerate J.T. active coordinate x and an inactive coordinate, which is now denoted by z, with harmonic force constants k and k_z, respectively:

$$V_{1,2}(x, z) = \frac{k}{2}(x \pm R_0)^2 + \frac{k_z}{2}(z - Z_0)^2 .$$

Case B: the two branches V_+ and V_- depend on two J. T. active coordinates x and y. In order to investigate the effect of an J. T. inactive mode in this case, too, we introduce a third coordinate z. However, for simplification we assume x, y to be degenerate (J. T. active e mode);

$$V_\pm(x, y, z) = \frac{k}{2}(\sqrt{x^2 + y^2} \pm R_0)^2 + \frac{k_z}{2}(z - Z_0)^2 .$$

Case A and this special case B may be looked at as limiting cases of a general case B with $k_x \neq k_y$ and $R_x \neq R_y$: then case A means $R_x = R_0$, $R_y = 0$ and case B $k_x = k_y$, $R_x = R_y$.

The Jahn-Teller energy ε, the difference between the potential minimum and the energy of the symmetric configuration (see Fig. 1), is given in both cases by

$$\varepsilon = \frac{k}{2} R_0^2 .$$

Furthermore, we want to investigate the influence of an additional spin-orbit interaction in an eletronic doublet state. The corresponding matrix element between the two adiabatic electronic states ψ_+, ψ_- constituing the ^2E may be approximated by

$$\langle \psi_+ | \boldsymbol{H}_{so} | \psi_- \rangle = i \frac{\lambda}{2} .$$

Then the adiabatic potential energies are

$$U_\pm(x, z) = \frac{k}{2}(x^2 + R_0^2) \pm \sqrt{(k R_0 x)^2 + \frac{\lambda^2}{4}} + \frac{k_z}{2}(z - Z_0)^2$$

for case A, and

$$U_\pm(x, y, z) = \frac{k}{2}(r^2 + R_0)^2 \pm \sqrt{(k R_0 r)^2 + \frac{\lambda^2}{4}} + \frac{k_z}{2}(z - Z_0)^2$$

for case B, where we have introduced $r^2 = x^2 + y^2$.

In both cases, these are two separate non-intersecting surfaces (see Fig. 1).

3. Line Shapes of Electronic $A \rightarrow E$ Transitions for Case B

In this paragraph we will discuss the line shape of an ${}^2A \rightarrow {}^2E$ absorption spectrum at low temperatures. In this case the initial state is the lowest vibrational state of the electronic state A with an assumed potential curve

$$V_A(x, y, z) = \frac{k'}{2}(x^2 + y^2) + \frac{k'_z}{2} z^2 .$$

Usually the force constants of the initial and the final state will be somewhat different. However, as we need the lowest vibrational function only for the calculation of Franck-Condon factors, the results will not change significantly, if we use $k' = k$, and $k'_z = k_z$ instead, for computational reasons. The line shapes are calculated with an inherent line width of $2\omega_0$ for each vibronic component ($\omega_0 = \sqrt{k/M}$, M = reduced mass), so that the vibrational structure of the spectrum is smeared out.

Vibronic Splittings

At first we discuss the case $\lambda = Z_0 = 0$. Results for several values of the Jahn-Teller parameter ε are displayed in Fig. 2. We see, that the band shapes exhibit a more and more pronounced splitting, as the Jahn-Teller coupling increases. The two main peaks of this well known vibronic splitting of the absorption bands, may be interpreted as originating from transitions into the lower and upper

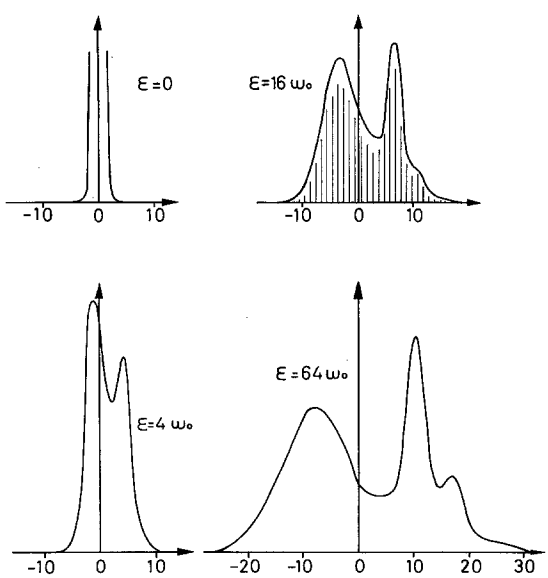

Fig. 2. Line shape of an electronic $A \rightarrow E$ transition at 0° K, calculated from $E \times e$ vibronic states. Natural line width $= 2\omega_0$, Jahn-Teller energy $\varepsilon = 0, 4, 16$ and $64\,\omega_0$. (For $\varepsilon = 16\,\omega_0$ single vibronic transition intensities are shown, too.)

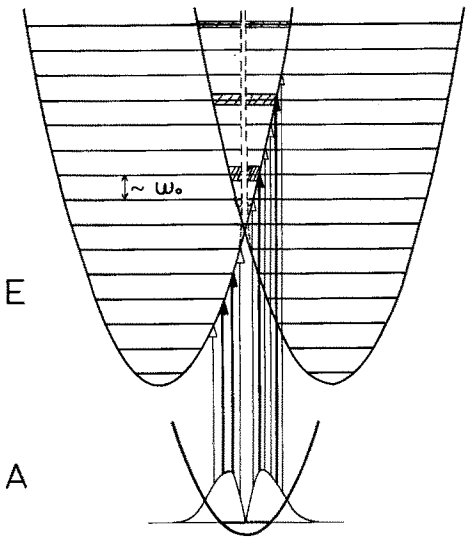

Fig. 3. $A \rightarrow E$ transitions in the configuration-coordinate model. —— adiabatic potential curves, – – – effective potential including the pseudocentrifugal term $\frac{1}{4\,Mr^2}$. —— vibronic levels, ≈≈≈≈ resonances in the inner potential well

well of the potential surface (see Fig. 3). A simple semiclassical model [2, 9] predicts two bands of equal shape centered at $E = 0$ and yields

$$\Delta E_{\text{vib}} = \sqrt{4\varepsilon\omega_0}$$

for the distance of the two maxima. Augmenting the adiabatic potential surface by a pseudocentrifugal term [2, 9] (see Fig. 3), the refined semiclassical model even yields the shift of the two bands to higher energies and a smaller width of the upper peak (see Fig. 2).

Furthermore we see from Fig. 2 that an increasing Jahn-Teller coupling leads to a further splitting of the absorption line shape. A third peak is fully developed at $\varepsilon = 64\,\omega_0$, on the right side of which we see an additional shoulder. Although neither the simple nor the refined semiclassical model is able to explain this phenomenon, we are nevertheless convinced that it is not merely an artifact of our calculational procedure: the basis sets of the numerical quantummechanical calculations have been expanded until the line shape did not change any more. Furthermore the results are reproducible with double precision arithmetic.

In order to investigate this new phenomenon, we will at first analyse the wave functions of the vibronic states. In the approximation used [5, 6] the vibronic wave functions are usually written as

$$\Psi = \psi_1(\xi) \cdot \chi_1(r, \phi) + \psi_2(\xi) \cdot \chi_2(r, \phi)$$

where ψ_1, ψ_2 are the two degenerate diabatic electronic wave functions depending on the electronic coordinates ξ only, and χ_1, χ_2 are the nuclear wave functions

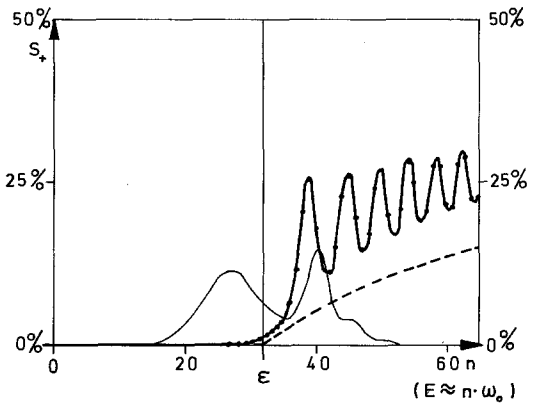

Fig. 4. Integrated density of vibronic $E \times e$ states associated with the upper part of the adiabatic potential surface versus vibronic main quantum number n ($\varepsilon = 32\,\omega_0$, $\lambda = 0$, $m = 0$), —— quantum mechanical result, - - - - classical approximation. —— absorption line shape of an $A \rightarrow E$ transition

depending on $r = \sqrt{x^2 + y^2}$ and $\phi = \text{arc tg}\, y/x$. Ψ may be transformed into[1]

$$\Psi = e^{i(m+\frac{1}{2})\phi} \cdot [\psi_+(\xi, \phi) \cdot \chi_+(r) + i\psi_-(\xi, \phi) \cdot \chi_-(r)]$$

where ψ_+, ψ_- are the adiabatic electronic wave functions corresponding to the upper and lower part of the adiabatic energy surface, and where the ψ's and χ's are real. From the normalization integral

$$1 = \langle \Psi | \Psi \rangle = \langle \psi_+ | \psi_+ \rangle \langle \chi_+ | \chi_+ \rangle + \langle \psi_- | \psi_- \rangle \langle \chi_- | \chi_- \rangle = S_+ + S_- .$$

one may calculate the percentages of the vibronic states, S_+ and S_-, associated with the upper and lower parts of the surface, respectively. The integrals needed are given in appendix A.

The result for $\varepsilon = 32\,\omega_0$ is shown in Fig. 4.

For energy values below ε, the system is nearly entirely on the lower part of the surface, for $E \gg \varepsilon$: $S_+ \rightarrow \frac{1}{2}$. This behaviour is to be expected from the classical model: the maximum probability is near the turning points, which are given by $r_t = R_0 \cdot \left(\sqrt{\frac{E}{\varepsilon}} \pm 1 \right)$. If we approximate S_+/S_- by the ratio of lengths of the lines of turning points in the x-y-plane, we obtain

$$S_+ = \begin{cases} 0 & \text{for} \quad E < \varepsilon \\ \frac{1}{2}\left(1 - \sqrt{\frac{\varepsilon}{E}}\right) & \text{for} \quad E > \varepsilon \end{cases}$$

which is plotted, too, in Fig. 4. (Refined classical models – e.g. using $1/p_\pm$ with $p_\pm = \sqrt{2M(E - U_\pm)}$ for the probability distribution function – do not lead to better quantitative agreement with the quantum mechanical result.)

[1] Only states with $m = 0$ may be reached by optical transitions from the vibrational groundstate of A [5].

However, contrary to the classical model, the quantum mechanical model shows pronounced oscillations of S_+ for $E > \varepsilon$. According to the Franck-Condon principle these should also show up in the line shape and explain the appearance of a third peak for large ε values. In Fig. 2, $\varepsilon = 64\,\omega_0$, and Fig. 4 ($\varepsilon = 32\,\omega_0$), we can even observe a further shoulder on the high energy side of the spectrum.

The maxima in the S_+-curve should correspond to metastable resonances in the upper potential well (see Fig. 3). As the well is very narrow (for $\varepsilon \gg \omega_0$) and extremely anharmonic, we expect that the energy spacings between the lowest levels are much larger than ω_0 and decrease with increasing quantum number. Furthermore, as the lowest states have their density maxima near the origin, they will lead to large Franck-Condon factors. Therefore, one might expect, that on the tail of the main progression (beginning at $E = \omega_0$, with rather harmonic spacings ω_0 and intensity maximum somewhat below $E = \varepsilon$) there is superimposed a second anharmonic progression with large spacings, with the first and most intense line somewhat above $E = \varepsilon$.

However, as the lowest states of the upper potential well are located near the branching point of the potential surface, they will show a large probability of changing over to the lower potential well. In other words, those states of the upper well, which give rise to strong transitions, will most strongly interact with the quasicontinuum of the broad lower well. Therefore we obtain only one single progression as shown for $\varepsilon = 16\,\omega_0$ in Fig. 2. This corresponds to the fact, that even for the second and third maximum, the probability of the final state to be on the inner part of the potential surface, is much smaller than 50% as is shown in Fig. 4.

Nevertheless, as the higher maxima in the absorption band are associated with the resonances in the upper well, their energy values E_n should be calculable from the quasiclassical quantisation rule:

$$\int_0^{r_t(E_n)} \sqrt{2M(E_n - (1 + r/R_0)^2)}\, dr = n\pi\,, \qquad n = 1, 2, 3 \ldots \tag{2}$$

Here we have omitted the pseudocentrifugal term of the potential in order to solve the integral in closed form, but have retained the restriction of the integration variable to positive values. Eq. (2) has been solved approximately in Appendix B. From there we obtain

$$\boxed{\Delta E \approx 1.65 \sqrt[3]{\varepsilon \omega_0^2}}$$

for the energy gap between the first two resonance states, which compares favourably well with the quantum mechanically calculated splitting between the second and third peaks of the spectra. The energy distance to the next maximum is somewhat smaller (see Fig. 4) and comes out to be $\Delta E \approx 1.39 \sqrt[3]{\varepsilon \omega_0^2}$.

From this discussion it is evident, that the additional vibronic splitting of the band shape is not an artifact of our simple model potential and should show up, too, in the case of more realistic ones, including higher order terms in the J. T. coupling, spin-orbit interaction and unharmonicity of the zero-order energy.

Effective Spin-Orbit Splitting

We now investigate the case where the spin-orbit coupling constant no longer vanishes. As is well known [7] and is evident from the adiabatic energy surfaces (see Fig. 1) the Jahn-Teller effect is suppressed by strong spin-orbit interaction. Similarly, a strong Jahn-Teller coupling quenches the spin-orbit coupling. The physical importance of this phenomenon was established by Ham [8] and is since then called the Ham-effect. The Ham-effect shows up e.g. in the reduced spin-orbit splitting of vibronic levels, if the Jahn-Teller coupling is switched on; this may be seen in a recent calculation of one of the authors (Figs. 3, 4 of

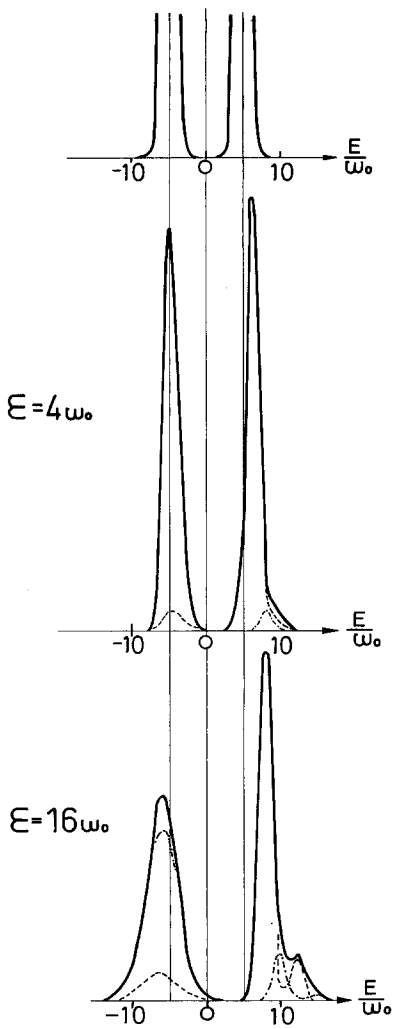

Fig. 5. Line shape of an electronic $^2A \rightarrow {}^2E$ transition at 0° K, calculated from $E \times e$ vibronic states. Natural line width $= 2\omega_0$, Jahn-Teller energy $\varepsilon = 0, 4, 16\,\omega_0$; spin-orbit splitting $\lambda = 10\,\omega_0$. The broken curves correspond to the intensities of the two spin-components

Ref. [6]). Contrary to this, we see from Fig. 5 that the effective spin-orbit splitting of a non-resolved vibrational band system becomes larger, if an additional Jahn-Teller coupling increases (see, too, Fig. 4 of Ref. [6]).

We have applied the simple semiclassical model to the case of nonvanishing spin-orbit coupling. One rather easily obtains for the peak distance

$$\Delta E_{\text{vib}+\text{so}} = \text{Max}\{\lambda; \sqrt{4\varepsilon\omega_0}\}$$

This obviously does not correspond to our quantum-mechanical result (Fig. 5), which can phenomenologically be described rather well by the equation

$$\boxed{\Delta E_{\text{vib}+\text{so}} = \sqrt{4\varepsilon\omega_0 + \lambda^2}} \tag{1}$$

This corresponds to a superposition of both the vibronic and spin-orbit splitting as two independent effects.

We also used the refined semiclassical model. However, it seems not to be possible to get a closed formula for the splitting, and the equations must be solved numerically. The results are in good agreement with the quantum-mechanical result as well as with the empirical Eq. (1).

Jahn-Teller Coupling and Vibrational Broadening

Finally we consider the case $Z_0 \neq 0$. We give a preliminary remark about the order of magnitude of Z_0: Let us describe the potential energy by some Valence Force Field model. In many cases, the J. T. active vibration is of the streching type or at least includes a marked bond stretching. Now, if the bond stretching parameters (i.e. bond lengths and valence force constants) will change upon electronic excitation to the degenerate E state, the parameters of all the stretching normal vibrations, including the a_{1g} mode, will change simultaneously.

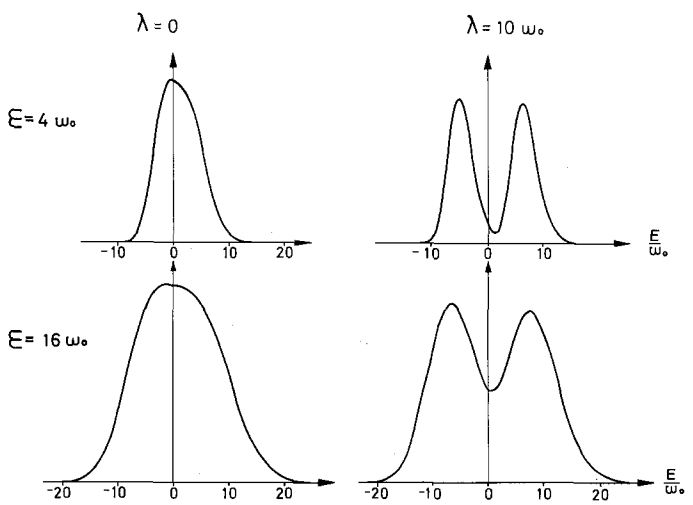

Fig. 6. Line shape of an electronic $^2A \rightarrow {}^2E$ transition at 0° K; $E \times e$ Jahn-Teller coupling (Jahn-Teller energy $= 4, 16\ \omega_0$) and a corresponding vibrational broadening by an a-mode; natural line width $2\ \omega_0$: spin-orbit splitting 0 and $10\ \omega_0$. Compare Fig. 2

(A special example is discussed in Chapter 5.) Therefore, the vibronic structure in the absorption line shape, caused by a strong dynamical J. T. effect in the upper state, will usually be smoothed by strong vibrational broadening due to the a_{1g} mode. As the additional splitting of the absorption line is much weaker than the main vibronic splitting we expect that the former one will usually be suppressed. Furthermore, at nonzero temperature hot bands will contribute, too, in this direction.

Line shapes for the case, where $k = k_z$ and $R_0 = Z_0$, are plotted in Fig. 6. Even the main vibronic splitting is smeared out, and we only obtain an asymmetric band with a shoulder on the high-energy side. Such line-shapes are experimentally realized e.g. in the spectra of many $Ti^{3+}L_6$-complexes [10], whereas in other cases (see e.g. Refs. [11]) line shapes are obtained which are intermediate between those of Figs. 2 and 6. No experimental spectra are known to us which are identical with those calculated without allowance for vibrational broadening by an a mode. Especially the only experimental hint for a third peak is supposed to be an artifact [11a]. Finally we remark that irrespective of an additional vibrational broadening the line-shape remains asymmetric and the effective splitting (that is the peak distance of two gaussians, into which the spectrum may be decomposed) is empirically given by the relation (1).

4. Line Shapes of Electronic $A \rightarrow E$ Transitions for Jahn-Teller Coupling Case A

In Fig. 7 we have drawn absorption line shapes of electronic $A \rightarrow E$ transitions with Jahn-Teller case A vibronic coupling. In the case of zero spin-orbit interaction we only observe vibrational broadening of the bands, but no asymmetry and no vibronic splitting as in case B.

As mentioned before, the adiabatic potential surfaces for case A and B are topologically equivalent, if we take a spin-orbit coupling into account. Therefore we except some similarity of case B band shapes and case A band shapes if $\lambda \neq 0$. And indeed, as is seen on the left side of Fig. 7, both phenomena are exhibited by the calculated $^2A \rightarrow {}^2E$ band shapes: a) the additional vibronic structure and b) the enhancement of the effective spin-orbit splitting by vibronic coupling. However, these vibronic effects only show up if there is strong spin-orbit interaction. And they are rather strongly suppressed by an additional a_{1g} vibrational broadening (see rhs. of Fig. 7). If R_0 and Z_0 are of comparable magnitude any asymmetry is no longer observable.

As for case B, the simple semiclassical model is not capable of reproducing the quantum mechanically calculated vibronic effects even qualitatively. On the other hand the refined semiclassical model predicts band shapes in rough agreement with Fig. 7. But we did not succeed in obtaining closed formulae for the splitting. Therefore we only give an empirical formula, which is fitted to the quantum mechanical results and reproduces them within $0.1\,\omega_0$ for parameter values in the range of $\lambda < 20\,\omega_0$ and $\varepsilon < 64\,\omega_0$:

$$\boxed{\Delta E_{\mathrm{so+vib}} = \sqrt{\lambda^2 + \omega_0 \cdot \sqrt[3]{20\,\lambda\varepsilon^2}}}$$

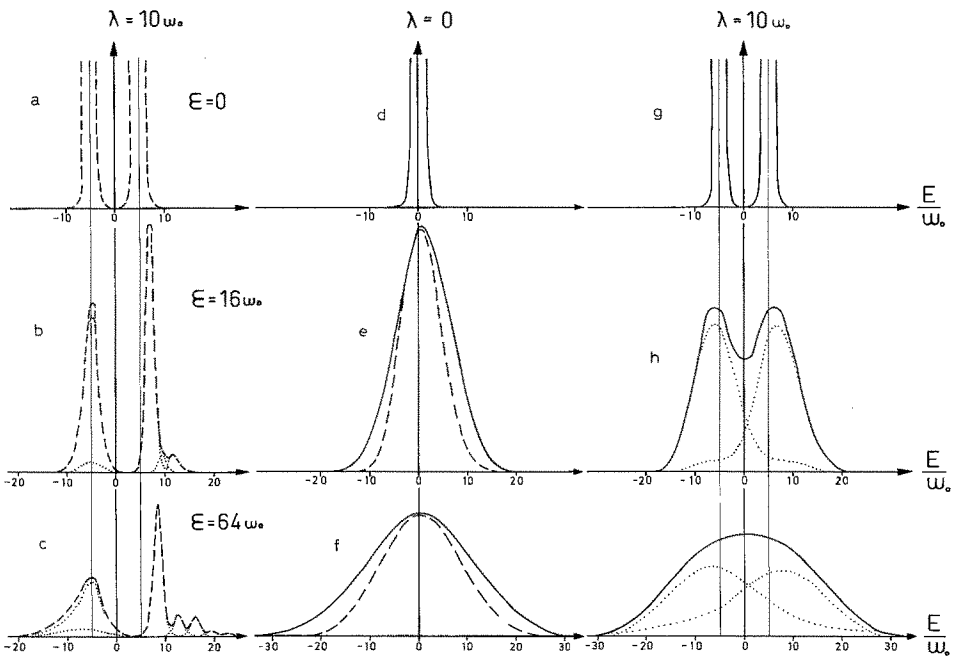

Fig. 7. Line shape of an electronic $^2A \rightarrow {}^2E$ transition at 0° K. $E \times b$ Jahn-Teller coupling case A. Broken curves without, full curves with an additional vibrational broadening ($Z_0 = R_0$). Jahn-Teller energy $\varepsilon = 0, 16, 64\,\omega_0$; spin-orbit splitting $\lambda = 0, 10\,\omega_0$; natural line width $2\,\omega_0$. The dotted curves correspond to the two spin-components of the transition

5. An Experimental Example

The presented investigation has been induced by difficulties in the interpretation of the main absorption lines in the XUV-spectrum of XeF_4 in the 200 Å region [13], which correspond to excitations of a xenon $4\,d_{3/2}$ or $4\,d_{5/2}$ electron into the lowest empty molecular orbital. XeF_4 has D_{4h} symmetry (see Fig. 8) and its LEMO is of e_u type. It may be approximated by xenon $5\,p_{x,y}$ – AO's, which are occupied in xenon itself but are nearly empty in the molecule because of the strong electronegativity of the fluorine ligands [14].

The spin-orbit splitting of the $4d$ level has been estimated to be 1.95 ± 0.01 eV and that of the e_u level to be about $0.6 - 0.7$ eV [13]. The possible four one-electron transitions are shown in Fig. 9. They are split and shifted by a) the field of the $F^{\delta-}$ ligands and b) the $4d$ hole-e_u electron interaction. The corresponding parameters have been estimated from results of a molecular SCF calculation [14]. The main transition energies and intensities then calculated are given in Table 2.

From this Table we see two deviations of the calculated from the measured values: 1) the splittings between peaks 1 and 2 and between peaks 3 and 4 are about 0.15 eV larger than calculated on the basis of an e_u spin-orbit splitting of 0.7 eV; 2) peak 4 is calculated so weak that it would not at all be observable. Now the two xenon $5p$ – AO's correlate with the σ_u-LEMO's of the $F_1 - F_3$ and $F_2 - F_4$ entities (see Fig. 8) and, therefore, are strongly antibonding. From our

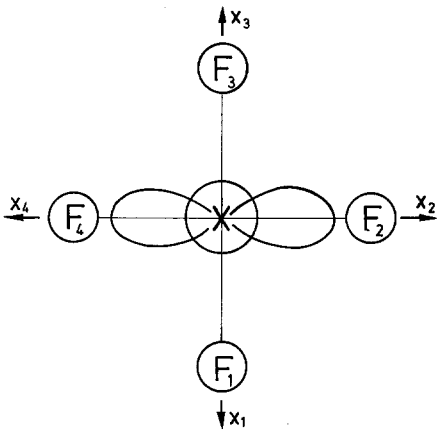

Fig. 8. Planar XF_4-molecule with D_{4h}-symmetry

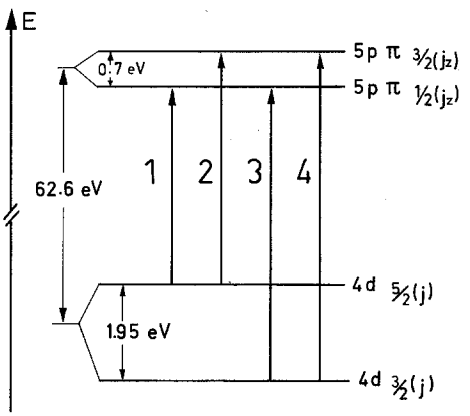

Fig. 9. One-electron levels engaged in the 60–65 eV excitations of XeF_4

Table 2. Xenon $4d \rightarrow$ "$5p$" transitions in XeF_4

Peak	Relative energy values in eV[a]			Relative intensities referring to a total of 2		
	Measured	Calculated		Measured	Calculated	
		With J. T. E.	Without J. T. E.		With J. T. E.	Without J. T. E.
1	−1.50	−1.52	−1.45	0.35	0.38	0.33
2	−0.40	−0.36	−0.45	0.65	0.63	0.68
3	0.70	0.70	0.77	0.7	0.82	0.95
4	1.50	1.49	1.40	0.3	0.17	0.04

[a] The energy values refer to the center of gravity.

experience with XeF_2 [13] we expect an expansion of the corresponding Xe-F equilibrium distance of about $R_0 = 1/3$ Å leading to D_{2h} symmetry. This should give rise to a dynamical Jahn-Teller effect in the absorption spectrum.The A_{1g} ground state of XeF_4 shows 7 normal vibrations: three bond stretching ones

(a_{1g}, b_{2g}, e_u), two in-plane bending ones (b_{1g}, e_u; the latter one is mixed to only a small degree with the e_u stretching mode [15]) and two out of plane bending ones (a_{2u}, b_{1u}). We expect that in the excited state only the bond lengths but not the equilibrium bond angles will be changed. Therefore the equilibrium values of the stretching symmetry coordinates only will change upon excitation. Furthermore, none of the bending modes will correlate with a_g under D_{2h} symmetry. Consequently there will occur no progressions of bending vibrations to any appreciable extent. This especially holds for the J. T. active b_{1g} mode and means that our problem is an example of J. T. case A. As the $4d-e_u$ hole-electron interaction is rather weak [13], we may treat the excitations within the one-electron picture, that is the transitions may be looked at as ${}^2A_{1g}\rightarrow{}^2E_u$ (and ${}^2E_g\rightarrow{}^2E_u$) transitions.

If we restrict ourselves to the internal stretching coordinates x_1, x_2, x_3, x_4 (see Fig. 8) and use the Modified Valence Force Field model, which is described in appendix C, the calculation leads to results which are also given in Table 2. We see that the theoretical energy splittings and the intensity values of peaks 3 and 4 are significantly improved, if the Jahn-Teller coupling is included. Furthermore the calculation with the parameters as chosen above reproduces the measured half width's of the absorption lines of about 0.7 eV [14].

The parameter values are near those of Fig. 7h: Each of the four one-electron transitions in XeF_4 roughly corresponds to one of the broken curves of Fig. 7h. They show the enhancement of the effective spin-orbit splitting by J. T. coupling and account for the energy difference of 0.15 – 0.2 eV mentioned at the beginning of this chapter. According to the mixing of pure spin-orbit states by the J. T. coupling, the broken curves exhibit a second shoulder which considerably contribute to the intensity of the two weak peaks 1 and 4.

6. Appendix

A. Calculational Details

All the quantum mechanical calculations have been performed numerically on an IBM 370 computer in a basis set of two- or three-dimensional harmonic oscillator functions. Most of the occuring integrals over generalized Laguerre polynomials $L_k^m(x)$ may be found in Refs. [5, 16]. Furthermore for the calculation of S_+-values (see chapter 3) one needs the integrals

$$S_{\mu\nu}=\int_0^\infty \frac{1}{\left(\frac{\mu-1}{2}\right)!}\cdot e^{-\frac{r^2}{2}}\cdot L^0_{\frac{\mu-1}{2}}(r^2)\times\frac{r}{\frac{\nu}{2}!\sqrt{\frac{\nu}{2}}}\cdot e^{-\frac{r^2}{2}}\cdot L^0_{\frac{\nu}{2}}(r^2)\times r\,dr$$

with μ odd and ν even. For these quantities, we obtained

$$S_{\mu\nu}=\sqrt{\frac{\pi}{2\nu}}(-1)^{\frac{\mu+\nu+1}{2}}\cdot\sum_{r=0}^{s}(-1)^r\cdot\prod_{t=0}^{\frac{\mu-1}{2}-r}\left(\frac{1.5}{t}-1\right)\cdot\prod_{t=1}^{\frac{\nu-2}{2}-r}\left(\frac{0.5}{t}-1\right)\cdot\prod_{t=1}^{r}\left(\frac{-0.5}{t}-1\right)$$

with s the smaller of the two integers $\frac{\mu-1}{2}$ and $\frac{\nu-2}{2}$. The products over t are to be set equal to unity, if their upper limit is zero.

For the calculation of the intensities we need the following integrals over the ususal harmonic oscillator functions $\varphi_n(z)$:

$$\int_{-\infty}^{+\infty} \varphi_0(z)\cdot\varphi_n(z+Z_0)\cdot dz = \sqrt{\frac{\eta^n}{n!}e^{-\eta}}$$

with $\eta = \frac{k_z}{2\omega_z} Z_0^2$. This result is obtained using the relation

$$\langle\varphi_0|Z^l|\varphi_n\rangle = \begin{cases} \dfrac{l!}{\sqrt{n!(2k_z/\omega_z)^l}\cdot 2^{\frac{l-n}{2}}\cdot\left(\frac{l-n}{2}\right)!} & \text{if } l-n \text{ even and non-negative} \\ \text{zero otherwise.} & \end{cases}$$

B. Quasiclassical Energy Levels

Solving the integral of Eq. (2), one obtains after substitution by $\arcsin x = \frac{\pi}{2} - \arcsin\sqrt{1-x^2}$

$$\pi n\,\omega_0 = E_n\left(\arcsin\sqrt{1-\frac{\varepsilon}{E_n}} - \sqrt{\frac{\varepsilon}{E_n}\left(1-\frac{\varepsilon}{E_n}\right)}\right).$$

We are interested in the E_n-values for small n, for which $\delta = \sqrt{\frac{E_n}{\varepsilon}} - 1 \ll 1$. In terms of δ, the equation reads

$$\frac{\pi n\,\omega_0}{\varepsilon} = (1+\delta^2)\cdot\arcsin\sqrt{\frac{\delta^2}{1+\delta^2}} - \delta \approx \frac{2}{3}\delta^3 - \frac{2}{15}\delta^5 + O(\delta^7).$$

If we retain only the first term of the power series, which is justified in the case of small δ, that is small n and large ε, the equation can be solved approximately for the E_n:

$$E_n = \varepsilon\left[1+\left(\frac{3\pi n}{2}\,\frac{\omega_0}{\varepsilon}\right)^{2/3}\right].$$

C. Bond stretching MVFF *for* XeF_4

$x_i (i = 1, 2, 3, 4)$ are the internal stretching coordinates of XeF_4 as indicated in Fig. 8. The potential energy of the A_{1g} ground state of XeF_4 is then written as

$$V(A_{1g}) = \frac{k}{2}\sum_{i=1}^{4} x_1^2 + \frac{k'}{2}\sum_{i=1}^{4} x_i(x_{i+1}+x_{i+2}+x_{i+3}).$$

In terms of symmetry coordinates,

$$\begin{aligned} \alpha_{1g} &= \tfrac{1}{2}(x_1 + x_2 + x_3 + x_4) \\ \beta_{2g} &= \tfrac{1}{2}(x_1 - x_2 + x_3 - x_4) \\ \varepsilon_{u1} &= \tfrac{1}{2}(x_1 - x_3) \quad \varepsilon_{u2} = \tfrac{1}{2}(x_2 - x_4)\,, \end{aligned} \tag{3}$$

this reads as

$$V(A_{1g}) = \frac{k+2k'}{2}\alpha_{1g}^2 + \frac{k}{2}\beta_{2g}^2 + \frac{k-k'}{2}(\varepsilon_{u1}^2 + \varepsilon_{u2}^2)$$

leading to the following normal frequencies

$$\begin{aligned} \omega(a_{1g}) &= \sqrt{(k+2k')/M_F} \\ \omega(b_{2g}) &= \sqrt{k/M_F} \\ \omega(e_u) &= \sqrt{(k-k')\,(1-2M_F/M_{Xe})/M_F}\,. \end{aligned}$$

M_F and M_{Xe} are the masses of the atoms F and Xe, respectively. With the force constants $k = 3.12 \dfrac{\text{mdyn}}{\text{Å}}$ and $k' = \dfrac{k}{20}$ the measured values [15] can be reproduced nearly exactly. We now approximate the potentials of the excited E_u state by

$$V_1(E_u) = \frac{k}{2}[x_1^2 + x_3^2] + \frac{\tilde{k}}{2}[(x_2 - R_0)^2 + (x_4 - R_0)^2] + \frac{k'}{2}\sum_{i=1}^{4} x_i(x_{i+1} + x_{i+2} + x_{i+3})$$

$$V_2(E_u) = \frac{k}{2}[x_2^2 + x_4^2] + \frac{\tilde{k}}{2}[(x_1 - R_0)^2 + (x_3 - R_0)^2] + \frac{k'}{2}\sum_{i=1}^{4} x_i(x_{i+1} + x_{i+2} + x_{i+3})$$

where we have assumed, that the small coupling force constant k' as well as the force constant k of the Xe-F bonds, not directly engaged with the excited electron, have not changed. Transformation to the coordinates given by Eqs. (3) yields (despite a constant term)

$$V_{1,2}(E_u) = \frac{k_\alpha}{2}(\alpha_{1g} - \varrho_\alpha) + \frac{k_\beta}{2}(\beta_{2g} \mp \varrho_\beta) \pm \Lambda \cdot \alpha_{1g} \cdot \beta_{2g} + \frac{k-k'}{2}\varepsilon_{u\,1,2}^2 + \frac{\tilde{k}-k'}{2}\varepsilon_{u2,1}^2$$

with

$$k_\alpha = \frac{k+\tilde{k}}{2} + 2k'\,, \qquad k_\beta = \frac{k+\tilde{k}}{2}$$

and

$$\varrho_\alpha = \frac{\tilde{k}}{k_\alpha}R_0\,, \qquad \varrho_\beta = \frac{\tilde{k}}{k_\beta}R_0\,.$$

From our model, which will be correct to first order, we see, that only the a_{1g} and b_{2g} vibrational modes are strongly influenced by the electronic excitation, whereas the e_u mode is only slightly split (into b_{2u} and b_{3u} of D_{2h}) by different force constants but does not exhibit a change in the equilibrium value.

We have calculated the absorption line shape from $E_u \times a_{1g} \times b_{2g}$ vibronic states using the parameters as given above and $\tilde{k} = 0.8\,k$. The final shape is not very sensitive to this latter choice.

Acknowledgement. We want to express our gratitude to Prof. Ballhausen, many comments of whom have greatly improved this manuscript.

The numerical calculations have been carried out on the IBM installation of the GMD at Bonn. We are grateful for computer time.

References

1. Jahn, H. A., Teller, E.: Proc. Royal Soc. (London) A**161**, 220 (1937).
2. Herzberg, G.: Molecular spectra and molecular structure, III. New York: Van Nostrand 1966; – Sturge, M. D.: Solid State Physics **20**, 91 (1967); – Ham, F. S.: In: Electron paramagnetic resonance, Ed. S. Geschwind. New York: Plenum Press 1971; Int. J. Quant. Chem. Symp. **5**, 191 (1971); – Englman, R.: The Jahn-Teller effect. London: Wiley 1972.
3. Ruch, E., Schönhöfer, A.: Theoret. chim. Acta (Berl.) **3**, 291 (1965).
4. Wagner, M.: Z. Physik **230**, 460 (1970).
5. Longuet-Higgins, H. C., Öpik, U., Pryce, M. H. L., Sack, H.: Proc. Royal Soc. (London) A**244**, 1 (1958); – Ballhausen, C. J.: Theoret. chim. Acta (Berl.) **3**, 368 (1965).
6. Schenk, H. J., Schwarz, W. H. E.: Theoret. chim. Acta (Berl.) **24**, 225 (1972).
7. Öpik, U., Pryce, M. H. L.: Proc. Royal Soc. (London) A**238**, 425 (1957).
8. Ham, F. S.: Physic. Rev. **166**, 307 (1968).
9. O'Brien, M. C. M.: Proc. physic. Soc. (London) **86**. 847 (1965).
10. Hartmann, H., Schläfer, H. L., Hansen, K. H.: Z. anorg. allg. Chem. **284**, 153 (1956); **289**, 40 (1957); – Pittel, B., Schwarz, W. H. E.: Ber. Bunsenges. **76**, 1025 (1972).
11. Cotton, F. A., Meyers, M. D.: J. Amer. chem. Soc. **82**, 5023 (1960); – Jones, G. D.: Physic. Rev. **155**, 259 (1967); – Freeman, T. F., Jones, G. D.: Physic. Rev. **182**, 411 (1969).
12. Vekhter, B. G., Tsukerblat, B. S., Rosenfeld, Yu. B.: Theoret. chim. Acta (Berl.) **27**, 49 (1972).
13. Comes, F. J., Haensel, R., Nielsen, U., Schwarz, W. H. E.: J. chem. Physics **58** (1973).
14. Basch, H., Moskowitz, J. W., Hollister, C., Hankin, D.: J. chem. Physics **55**, 1922 (1971).
15. Tsao, P., Cobb, C. C., Claassen, H. H.: J. chem. Physics **54**, 5247 (1971).
16. Schrödinger, E.: Ann. Physik **80**, 483 (1926).

Dr. E. Schwarz
Lehrstuhl für Theoretische Chemie
der Universität Bonn
D-5300 Bonn
Wegelerstr. 12
Federal Republic of Germany